Broadband acoustic focusing by symmetric Airy beams with phased arrays comprised of different numbers of cavity structures*

Jiao Qian(钱姣)[1,‡], Bo-Yang Liu(刘博阳)[1,‡], Hong-Xiang Sun(孙宏祥)[1,2,†]
Shou-Qi Yuan(袁寿其)[1,‡], and Xiao-Zhu Yu(俞笑竹)[1]

[1] *Research Center of Fluid Machinery Engineering and Technology, Faculty of Science, Jiangsu University, Zhenjiang* 212013, *China*
[2] *State Key Laboratory of Acoustics, Institute of Acoustics, Chinese Academy of Sciences, Beijing* 100190, *China*

(Received 29 July 2017; revised manuscript received 9 September 2017; published online 16 October 2017)

We realize broadband acoustic focusing effect by employing two symmetric Airy beams generated from phased arrays, in which the units of the phased arrays consist of different numbers of cavity structures, each of which is composed of a square cavity and two inclined channels in air. The exotic phenomenon arises from the energy overlapping of the two symmetric Airy beams. Besides, we demonstrate the focusing performance with high self-healing property, and discuss the effects of structure parameters on focusing performance, and present the characteristics of the cavity structure with straight channels. Compared with other acoustic lenses, the proposed acoustic lens has advantages of broad bandwidth (about 1.4 kHz), high self-healing property of focusing performance, and free adjustment of focal length. Our finding should have great potential applications in ultrasound imaging and medical diagnosis.

Keywords: acoustic focusing, Airy beam, phase manipulation, cavity structure

PACS: 43.35.+d, 43.25.+y **DOI:** 10.1088/1674-1056/26/11/114304

1. Introduction

Acoustic focusing has extensive applications in many scenarios ranging from biomedical imaging to therapeutic ultrasound to non-destructive evaluation.[1–6] Conventional acoustic focusing lenses are designed by bending natural materials into specific shapes to change acoustic propagation paths, which inevitably leads to inherent geometrical and wave aberrations. The rapid expansion of sonic crystals (SCs)[7,8] and acoustic metamaterials[9–12] offers extreme acoustic parameters unattainable with natural materials, which provide alternative solutions to acoustic lenses design. The SCs have been adopted to design acoustic lenses with sound gradient-refractive indexes.[13–15] However, the sizes of these types of the lenses are large at low frequency. With the emergence of acoustic metamaterials,[16–19] a small and thin acoustic focusing lens has become possible, owing to the small size and large negative refractive index of unit. Recently, acoustic metasurfaces enable the design of planar acoustic lens with phase manipulation,[20–31] which is different from other acoustic lenses. Besides, the thickness of the planar lens is much smaller than its working wavelength, which markedly increases the potential for the integration of the acoustic lenses. In addition to the aforementioned lenses, we have realized the acoustic focusing lenses by using the thermoacoustic mechanism[32–35] and the acoustic metafiber,[36] which have advantages of high focusing performance and broad working bandwidth.

Despite the improvement of the focusing performance and device structure by using the SCs, the acoustic metamaterials and metasurfaces, the existing focusing mechanisms are inevitably affected by various scatterers in acoustic focusing paths. As a typical example, the influences of ribs on the focusing effect in the high intensity focused ultrasound (HIFU) treatment seriously restrict the treatments of deep-seated tumors inside the ribcage. Aiming at this problem, Gao *et al.*[29] proposed a new type of acoustic focusing lens based on symmetric self-bending beams with phase manipulations, which could circumvent scatterers in focusing paths. However, the acoustic lens is composed of a phased array with zero-index medium, which results in the narrow working bandwidth of the lens. However, in practical therapeutic ultrasound, it is highly desirable to effectively focus acoustic waves in a broad bandwidth in the presence of scatterers, which requires exploring the inherently distinct mechanism of acoustic focusing.

In this work, we propose a broadband acoustic focusing lens which consists of two symmetric phased arrays of Airy beam in air. The unit of the phased arrays is realized by using different numbers of cavity structures each of which is composed of a square cavity and two inclined channels, which has advantages of the easy fabrication and the flexible operation. The focusing effect is attributed to the energy over-

*Project supported by the National Natural Science Foundation of China (Grant Nos. 11774137 and 11404147), the Major Program of the National Natural Science Foundation of China (Grant No. 51239005), the Natural Science Foundation of Jiangsu Province, China (Grant Nos. BK20140519 and BK20140523), the Jiangsu Qing Lan Project, China, and the Practice Innovation Training Program Projects for Industrial Center of Jiangsu University, China.

‡Jiao Qian and Bo-Yang Liu contributed equally to this work.
†Corresponding author. E-mail: jsdxshx@ujs.edu.cn
‡Corresponding author. E-mail: shouqiy@ujs.edu.cn

© 2017 Chinese Physical Society and IOP Publishing Ltd

lapping of the two symmetric Airy beams. Furthermore, we demonstrate the self-healing property of the acoustic lens and discuss the effects of structure parameters on focusing performance in detail.

2. Numerical model and design scheme

2.1. Units of phase manipulation

As shown in Fig. 1, a cavity structure (red dash rectangle) consists of a square cavity with two symmetric inclined channels immersed in air. The length (h) and width (d) of the cavity structure are 20 mm and 7 mm, respectively, and the length (l) of the solid structure is 12 mm. The length (a) of the square cavity, the width (w) and the inclined angle (θ) of the channel are 5 mm, 2 mm, and 58°, respectively. The solid structure is made of photosensitive resins to satisfy the sound hard boundary condition. Throughout this work, the finite element method based on COMSOL Multiphysics software is utilized to numerically simulate the performances of acoustic waves. The material parameters are adopted as follows: the density $\rho = 1180$ kg/m^3, the longitudinal wave velocity $c_l = 2720$ m/s, and the transversal wave velocity $c_t = 1460$ m/s for epoxy resin; $\rho = 1.21$ kg/m^3 and $c_l = 343$ m/s for air.

Figure 2(a) shows the numerical model for the transmission spectra and the transmitted phase delays of n-layers cavity structures, in which the incident acoustic source is located at the left boundary of the model. The transmission spectra are shown in Fig. 2(b) for the numbers of the cavity structures (n) of 1, 2, 3, 4, 5, and 6, respectively. It is found that with the increase of n, the transmission spectra are almost the same. In the range of 7.4 kHz–9.1 kHz, the transmission is larger than 0.7. Therefore, the cavity structure has a broad working bandwidth. Figure 2(c) shows the distribution of the transmitted phase delays as a function of n at 7.95 kHz, in which the phase delays of six blue hollow dots are about $\pi/3$, $2\pi/3$, π, $4\pi/3$, π, $5\pi/3$, and 2π, which correspond to the units with $n = 1$, 2, 3, 4, 5, and 6, respectively. Note that the phase delay gradually increases with the increase of n, and could span entire 2π range when n increases to 6. Thus, we can arbitrarily manipulate the acoustic propagation paths by changing the number of the cavity structures. Compared with other types of units,[20,21,24] the proposed units of phase manipulation have advantages of the easy fabrication and the flexible operation.

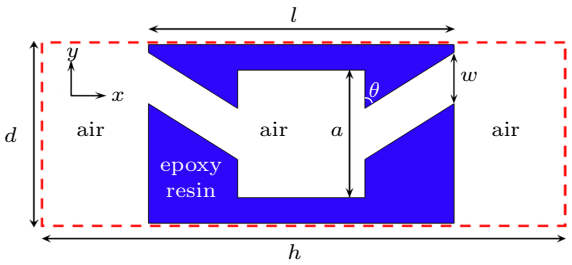


Fig. 1. (color online) Schematic of cavity structure.

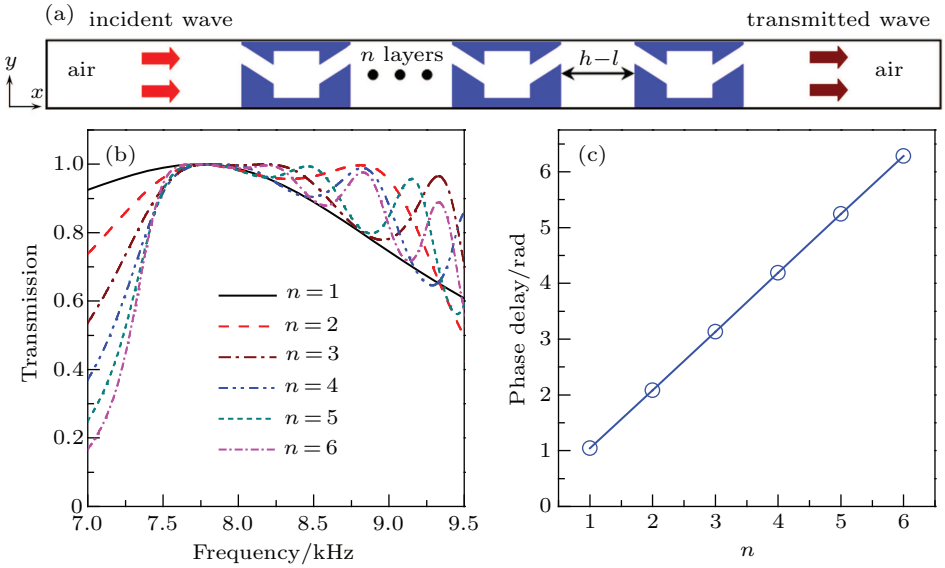


Fig. 2. (color online) (a) Schematic of numerical model for transmission spectra and phase delays of units, (b) transmission spectra, and (c) phase delay versus the number of units.

2.2. Design method of acoustic focusing lens

Considering the acoustic waves with normal incidence along the x direction and the presence of discrete phase delays along the y direction, the refraction angle of the transmitted wave θ_t (measured from the x direction) can be obtained by using the generalized Snell's law[37]

$$\sin\theta_t = \frac{1}{k}\frac{\mathrm{d}\varphi(y)}{\mathrm{d}y}, \tag{1}$$

where $\varphi(y)$ represents the phase delay along the y direction, $k = 2\pi f/c$ is the wave vector in air, with c and f being the acoustic velocity and the frequency, respectively. Based on Eq. (1), the acoustic propagation path can be manipulated arbitrarily by changing the distribution of the phase delays along the y direction. To realize an acoustic Airy beam, the distribution of the phase delays along the y direction satisfies[29]

$$\varphi(y) = \arg[\mathrm{Ai}(by)\exp(ay - \mathrm{i}kby\sin\theta)], \tag{2}$$

where Ai(by) is the Airy function, b represents the transverse scale, the value of a is positive so as to ensure the energy is finite, and θ is the bending angle of the Airy beam. In the work, we design an acoustic focusing lens composed of two phased arrays of the Airy beam, symmetric with respect to $y = 0$. Owing to the self-bending property of the Airy beam, two Airy beams generated from two symmetric phased arrays are focused on their overlapping region.

3. Numerical results and discussion

3.1. Focusing performance

In the phased array of the Airy beam, the parameters a, b, θ, f, and c are selected as 0.5, 22, 0.5°, 7.95 kHz, and 343 m/s, respectively. The theoretical continuous phase delays along the y direction are shown as the blue solid line in Fig. 3(a). Based on the phase delays of the six units in Fig. 2(c), we design a phased array for the Airy beam provided by 151 discrete phase delays (red hollow dots) along the y direction. Figures 3(b) and 3(c) show the distributions of the acoustic intensity field for the Airy beam with the theoretical continuous phase delays and the phased array, respectively. The results of the two cases agree well with each other, which demonstrates the feasibility of the proposed phased array of the Airy beam. As shown in Fig. 3(c), the acoustic Airy beam generated from the phased array shows the self-bending property and has no diffraction in the far-field region. Besides, the energy of the Airy beam is localized spatially and mostly concentrated in the main lobe.

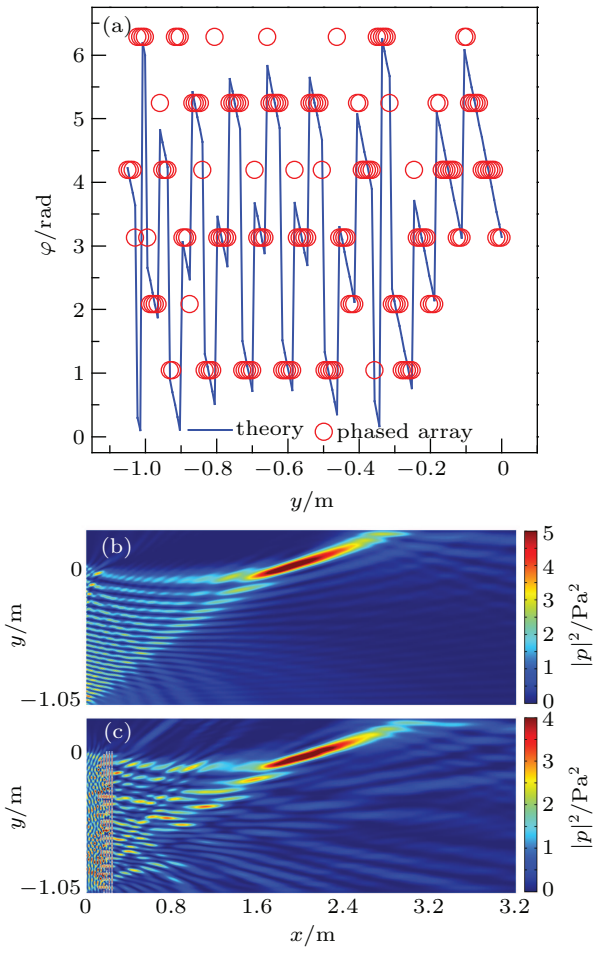


Fig. 3. (color online) (a) Theoretical continuous (blue line) and discrete phase delays (red hollow dots) provided by six types of units in Fig. 2(c) (blue hollow dots) for Airy beam. Spatial distributions of acoustic intensity field $|p|^2$ for Airy beam by using (b) theoretical continuous phase delays and (c) discrete phase array at 7.95 kHz.

On the basis of the phased array for the Airy beam, we design an acoustic focusing lens composed of two identical phased arrays symmetric with respect to $y = 0$. The distribution of the acoustic intensity field induced by the theoretical continuous phase delays and the proposed acoustic lens are shown in Figs. 4(a) and 4(b), respectively. It is noted that the focusing characteristic induced by the proposed acoustic lens agrees well with the theoretical result, which indicates that the acoustic focusing can be realized by using two symmetric Airy beams.

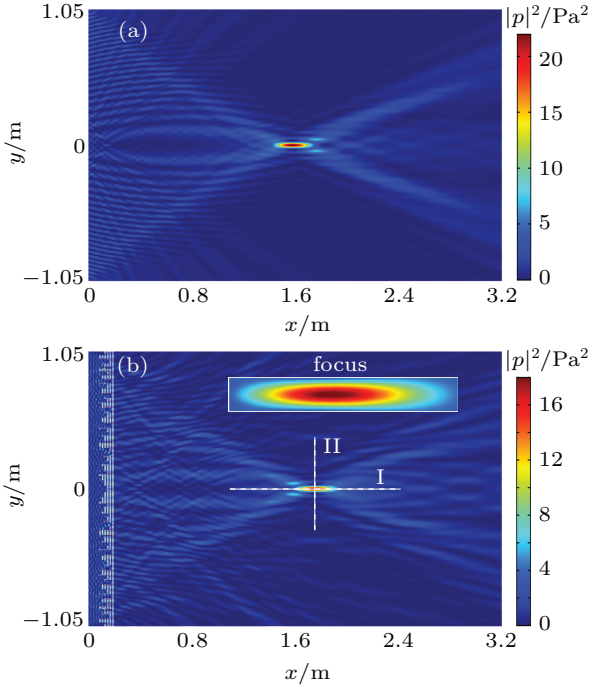


Fig. 4. (color online) Spatial distributions of acoustic intensity field induced by (a) theoretical continuous phase delays and (b) proposed acoustic lens at 7.95 kHz.

To quantify the performance of the acoustic lens, we calculate the longitudinal and transverse distributions of the acoustic intensity through the focus (shown as lines I and II in Fig. 4), which are shown in Figs. 5(a) and 5(b), respectively. The results in the free space are also exhibited there for comparison. It is found that the focusing effect exists in both x and y directions. Compared with the results in the free space, the acoustic intensity at the focus is enhanced by about 18 times in the case with the acoustic lens. It is deduced that the acoustic lens has good performance in both horizontal and vertical directions.

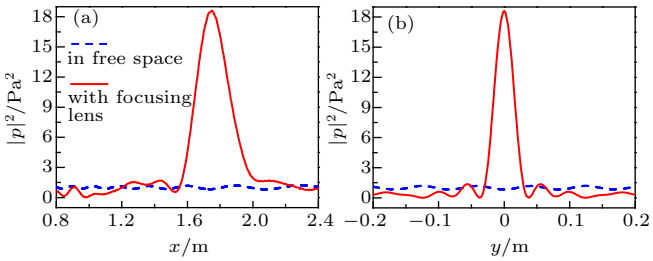


Fig. 5. (color online) Distributions of acoustic intensity through focus along lines (a) I and (b) II in Fig. 4.

3.2. Broad working bandwidth

The acoustic focusing of the proposed lens exists in a broad working bandwidth. Figures 6(a)–6(d) show the distributions of the acoustic intensity field induced by the acoustic lens at 7.6 kHz, 8.3 kHz, 8.65 kHz, and 9.0 kHz, respectively, in which the lens parameters are the same as those in Fig. 4. We find that the acoustic lens presents high focusing performances at these frequencies, which indicates that the working bandwidth of the acoustic lens increases up to 1.4 kHz. Besides, the focus moves toward the right with the increase of frequency. Figure 7 exhibits the transverse distributions of the acoustic intensity through the focus at these frequencies. It is also found that the position of the focus gradually moves toward the right with the increase of the frequency. Therefore, it is deduced that the proposed focusing lens has a broad working bandwidth, and the focal length can be controlled by adjusting the incident frequency, which is different from other acoustic lenses with symmetric Airy beams.[29]

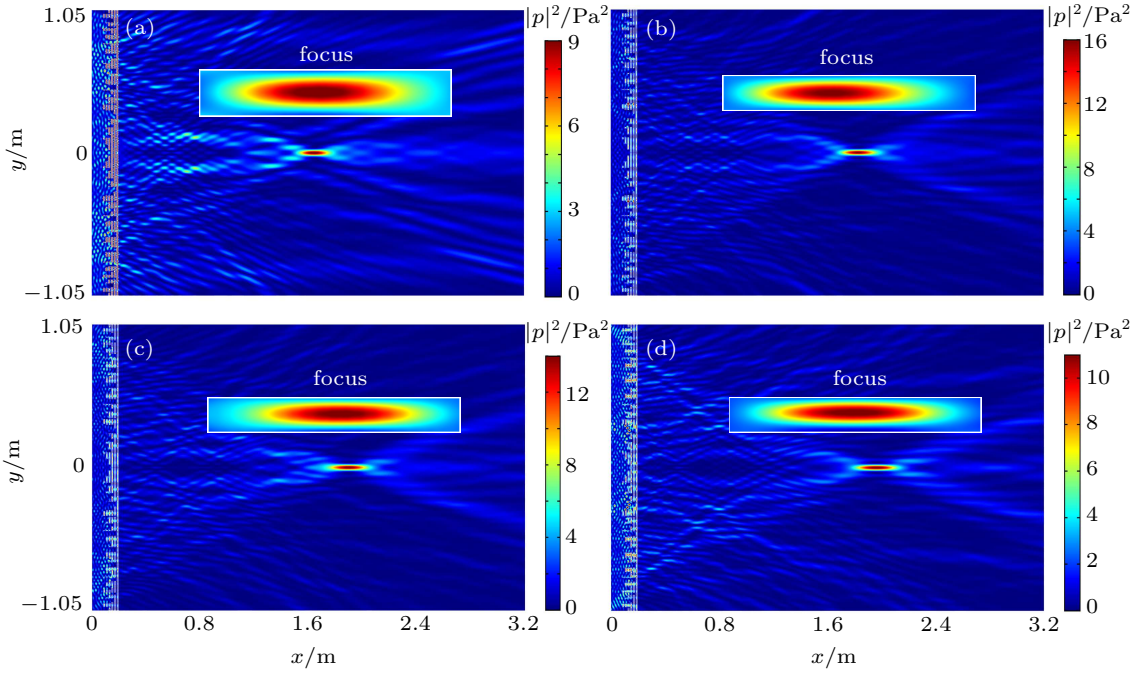


Fig. 6. (color online) Spatial distributions of acoustic intensity field induced by acoustic lens at (a) 7.6 kHz, (b) 8.3 kHz, (c) 8.65 kHz, and (d) 9.0 kHz.

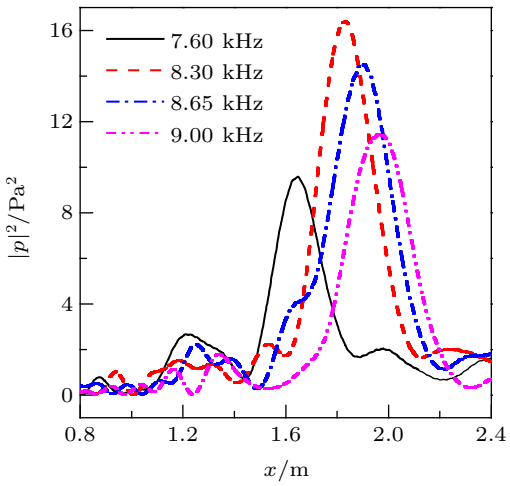


Fig. 7. (color online) Transverse distributions of acoustic intensity through focus for acoustic lens at different frequencies.

3.3. Focusing performance with self-healing property

In order to study the influence of a scatterer on the focusing performance, we place an elliptical scatterer on the acoustic focusing path. The distance between the center of the scatterer and the lens is 23 cm, and the semi-major and semi-minor axis of the ellipse scatterer are 15 cm and 9 cm, respectively. Figure 8 shows the distribution of the acoustic intensity field with the elliptical scatterer placed on the acoustic focusing path. As shown in Fig. 8, the transmitted acoustic energy can circumvent the elliptical scatterer and converge into a focal region. The focusing performance is almost the same as that in Fig. 4, which reveals the distinctive self-healing property of the focusing performance generated from the proposed acoustic lens.

To further verify this, we design a traditional acoustic focusing lens with the same length along the y direction. Theo-

retical continuous and discrete phase delays for the half structure of the traditional acoustic lens are shown as the blue solid line and red hollow dots in Fig. 9. Figures 10(a) and 10(b) show the distributions of the acoustic intensity field induced by the traditional acoustic lens without and with the elliptical scatterer placed on the focusing path, in which the parameters of the elliptical scatterer are the same as those in Fig. 8. It is found that the focusing effect exists clearly on the right side of the traditional acoustic lens. Compared with the results in Fig. 10(a), the acoustic intensity in the focus region decreases greatly in Fig. 10(b). Therefore, we deduce that the focusing performance of the traditional acoustic lens is significantly affected by the elliptical scatterer.

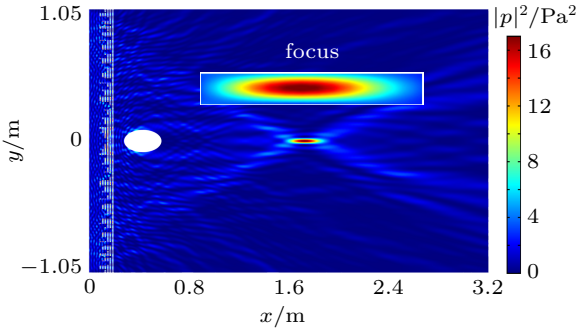


Fig. 8. (color online) Spatial distribution of acoustic intensity field induced by acoustic lens with elliptical scatterer placed on acoustic focusing path.

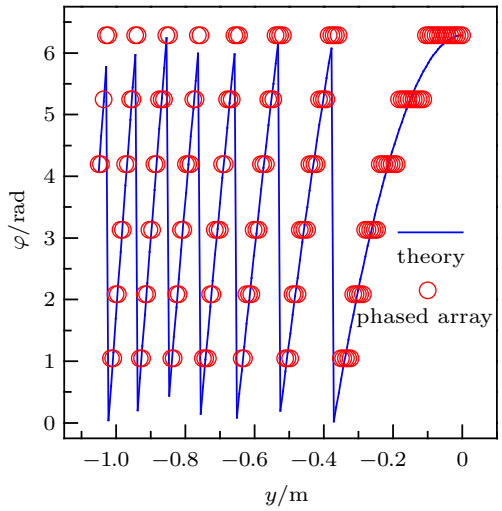


Fig. 9. (color online) Theoretical continuous phase delays (blue line) and discrete phase delays (red hollow dots) for half structure of traditional acoustic focusing lens.

Figure 11 shows the longitudinal distributions of the acoustic intensity through the focus for the traditional and proposed acoustic lenses with the elliptical scatterer, in which the results without the elliptical scatterer are also displayed for comparison. The intensities are normalized by the maximum of the intensities without the elliptical scatterer. It is shown from Figs. 11(a) and 11(b) that the maximum values of the normalized intensity are about 0.79 and 0.94 for the traditional and proposed acoustic lenses with the elliptical scatterer, respectively. The results further demonstrate the self-healing feature of the acoustic focusing of the proposed lens, which arises from the self-healing property of the Airy beam able to deliver most of the energy into the focus region.

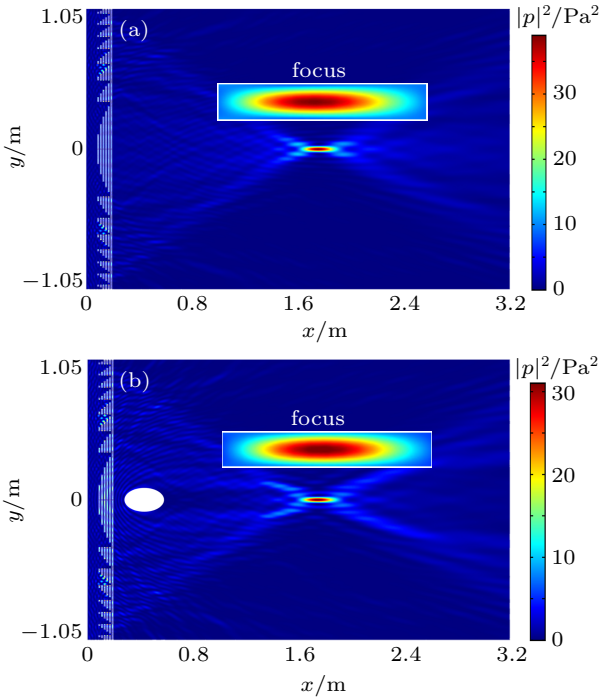


Fig. 10. (color online) Spatial distributions of acoustic intensity field induced by traditional acoustic lens (a) without and (b) with elliptical scatterer placed on acoustic focusing path at 7.95 kHz.

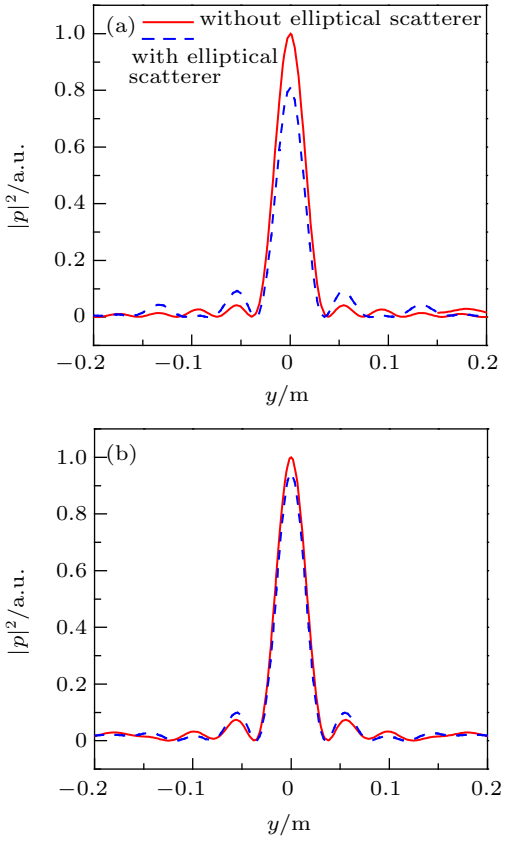


Fig. 11. (color online) Longitudinal distributions of acoustic intensity through focus for (a) traditional and (b) proposed acoustic lenses with elliptical scatterer.

3.4. Effects of structure parameters on focusing performance

We also discuss the influences of the structure parameters (θ and b) on the focusing performance. Figures 12(a)–12(c) show the distributions of the acoustic intensity field for the Airy beams with different values of θ, in which the values of parameter θ are selected as 0.3°, 0.4°, and 0.6°, respectively, and the other parameters remain constant. It is clearly shown that with the increase of θ, the curvature of the Airy beam decreases gradually and the main lobe of the Airy beam shifts toward the lower right.

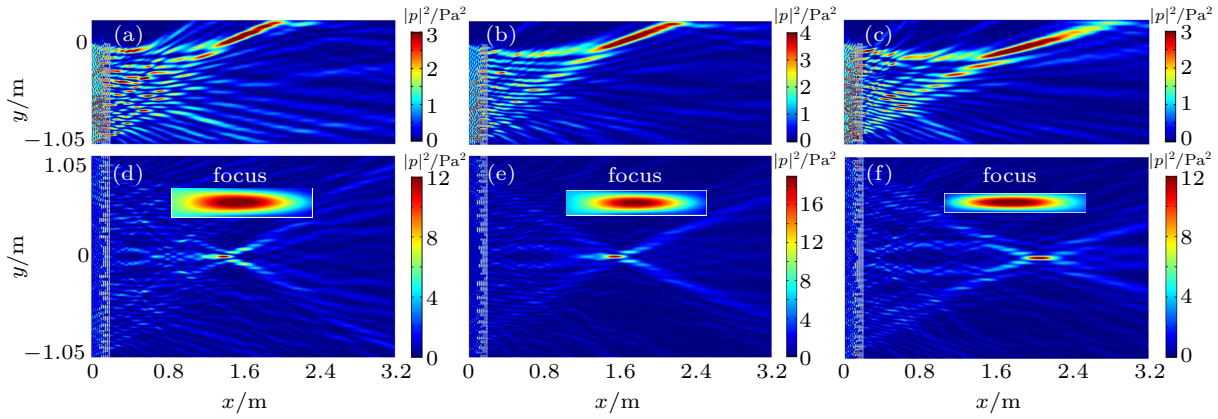


Fig. 12. (color online) Spatial distributions of intensity field for Airy beams with parameter (a) $\theta = 0.3°$, (b) 0.4°, and (c) 0.6°, and induced by acoustic lenses with parameter (d) $\theta = 0.3°$, (e) 0.4°, and (f) 0.6° at 7.95 kHz.

According to the phased arrays of the Airy beam in Figs. 12(a)–12(c), we design three types of acoustic lenses with different values of θ, and the distributions of the acoustic intensity field induced by the three types of the lenses are shown in Figs. 12(d)–12(f). It is found that the acoustic focusing also exists on the right side of these lenses, and the position of focus shifts toward the right gradually with the increase of θ. This is because the curvature of the Airy beam decreases gradually. The transverse distributions of the acoustic intensity through the focus with different values of θ are shown in Fig. 13. We find that the focus shifts toward the right with the increase of θ, which indicates that the focal length of the acoustic lens can be manipulated by adjusting the value of θ.

Figures 14(a)–14(c) present the distributions of the acoustic intensity field for the Airy beams with different values of b, i.e., 21, 23, and 24, and the other parameters are kept unchanged. It is found that the distance between the center of the main lobe and the phased array decreases gradually with the increase of b. According to the phased arrays for the Airy beam in Figs. 14(a)–14(c), we design three types of acoustic lenses with different values of b. The distributions of the acoustic intensity field induced by the acoustic lenses with different values of b are displayed in Figs. 14(d)–14(f).

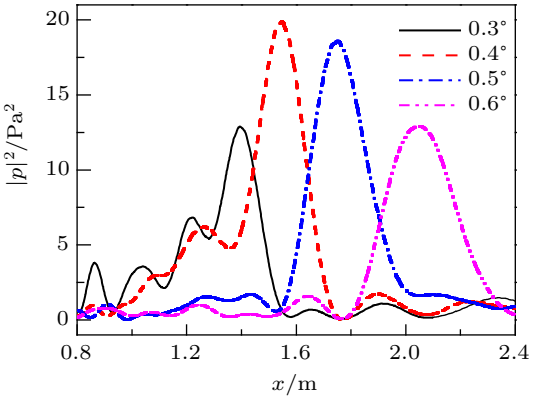


Fig. 13. (color online) Transverse distributions of acoustic intensity through focus for acoustic lenses with different values of parameter θ.

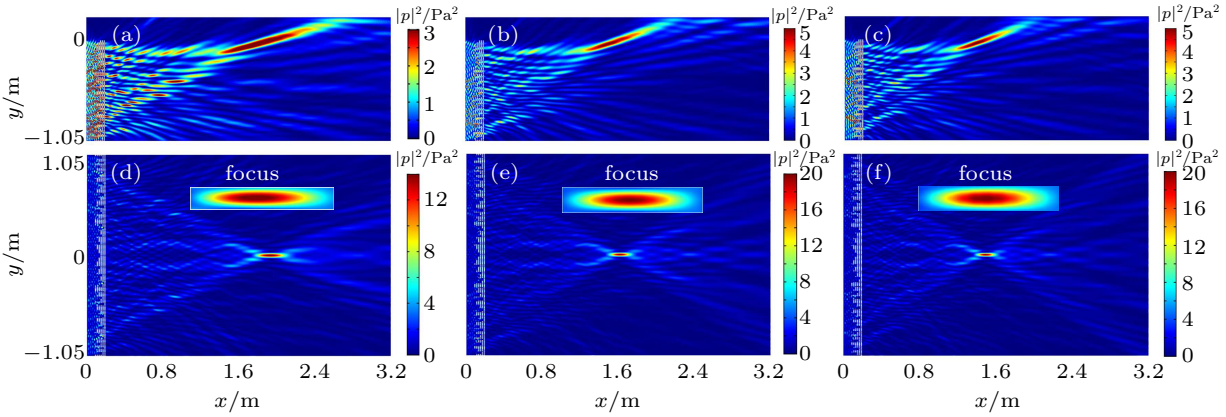


Fig. 14. (color online) Spatial distributions of intensity field for Airy beams with parameter (a) $b = 21$, (b) 23, and (c) 24 induced by acoustic lenses with parameter (d) $b = 21$, (e) 23, and (f) 24 at 7.95 kHz.

We find that with the increase of b, the focus shifts toward the left and the focal length gradually decreases, which arises from the decreasing of the distance between the main lobe and the phased array. In addition, we calculate the transverse distributions of the acoustic intensity through the focus with different values of b, which is shown in Fig. 15. It is also found that the focus shifts toward the left with the increase of b. Therefore, we deduce that the focal length of the acoustic lens can be controlled by the parameters θ and b.

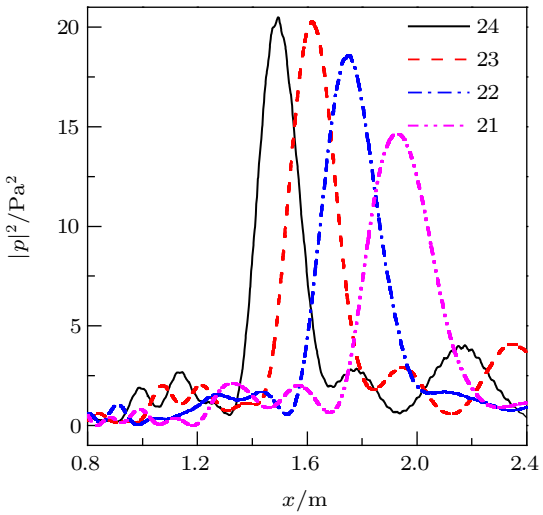


Fig. 15. (color online) Transverse distributions of acoustic intensity through focus for acoustic lenses with different values of parameter b.

3.5. Cavity structure with straight channels

To show the motivation of using the cavity structure with inclined channels, we calculate the characteristics of the cavity structure with two symmetric straight channels (Fig. 16) for comparison, and the other parameters remain constant. Figure 17(a) presents the transmission spectra with different numbers (n) of the cavity structure with straight channels. Compared with the results in Fig. 2(b), the working bandwidth shifts to the high frequency region and the transmissions all reach about l.0 at 8.8 kHz with $n = 1, 3, 5, 7$ and 9 in Fig. 17(a). Figure 17(b) shows the distribution of the transmitted phase delays as a function of n at 8.8 kHz. Note that the phase delay of this type of cavity structure spans entire 2π range when n increases to 9. Compared with the result in Fig. 2(c), the number of the cavity structure increases greatly, which leads to the designed focusing lens much thicker. Thus, we adopt the cavity structure with inclined channels to design the acoustic lens.

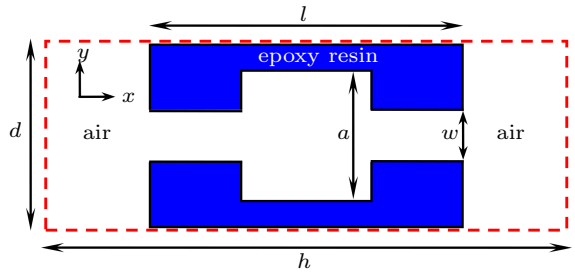


Fig. 16. (color online) Schematic of cavity structure with straight channels.

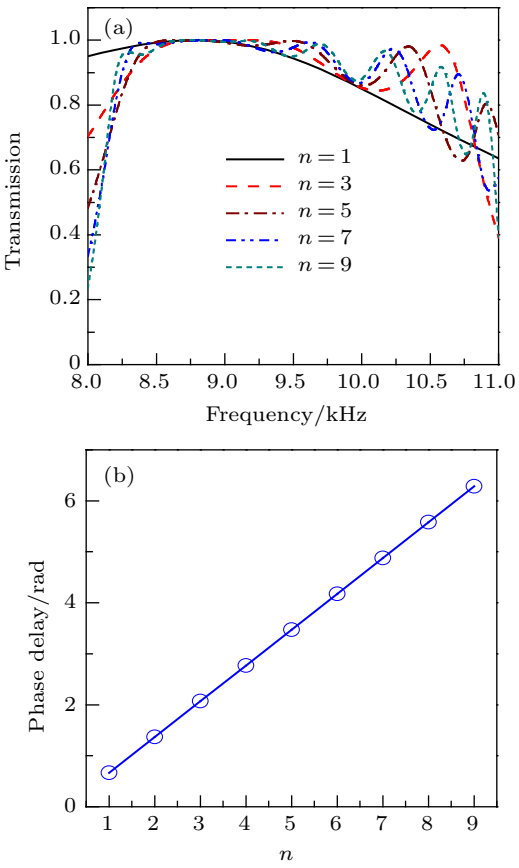


Fig. 17. (color online) (a) Transmission spectra and (b) transmitted phase delays with different numbers of cavity structure with straight channels.

4. Conclusions

In this study, we realize a broadband acoustic focusing effect through two symmetric phased arrays of Airy beam in air. The results show that the units of the phased arrays consist of different numbers of the cavity structures with inclined channels, which have advantages of easy fabrication and flexible operation. The phase delays of the units could span entire 2π range by using six cavity structures with inclined channels, which is less than those with straight channels. The focusing effect stems from the energy overlapping of the two symmetric Airy beams. Owing to the self-bending and self-healing features, the ability to circumvent a scatterer of the proposed acoustic lens is greater than that of traditional acoustic lenses. Moreover, the bandwidth of the focusing effect increases up to 1.4 kHz, and the focal length of the lens can be controlled by adjusting incident frequency and parameters θ and b. The above results provide the theoretical basis for designing broadband acoustic focusing lenses, which have great potential applications in ultrasound imaging and medical diagnoses.

References

[1] Zhao J J, Ye H P, Huang K, Chen Z N, Li B W and Qiu C W 2015 *Sci. Rep.* **4** 6257
[2] Xia J P and Sun H X 2015 *Appl. Phys. Lett.* **106** 063505
[3] Gu Y, Cheng Y and Liu X J 2015 *Appl. Phys. Lett.* **107** 133503
[4] Xia J P, Sun H X, Cheng Q, Xu Z, Chen H, Yuan S Q, Zhang S Y, Ge Y and Guan Y J 2016 *Appl. Phys. Express* **9** 057301
[5] Guan Y J, Sun H X, Liu S S, Yuan S Q, Xia J P and Ge Y 2016 *Chin. Phys. B* **25** 104302

[6] Zheng L and Guo J Z 2016 *Acta Phys. Sin.* **65** 044305 (in Chinese)
[7] Liu Z Y, Zhang X X, Mao Y W, Zhu Y Y, Yang Z Y, Chan C T and Sheng P 2000 *Science* **289** 1734
[8] Lu J Y, Qiu C Y, Ke M Z and Liu Z Y 2016 *Phys. Rev. Lett.* **116** 093901
[9] Lai Y, Wu Y, Sheng P and Zhang Z Q 2011 *Nat. Mater.* **10** 620
[10] Liang Z and Li J 2012 *Phys. Rev. Lett.* **108** 114301
[11] Xie Y B, Wang W Q, Chen H Y, Konneker A, Popa B I and Cummer S A 2014 *Nat. Commun.* **5** 5553
[12] Cheng Y, Zhou C, Yuan B G, Wu D J, Wei Q and Liu X J 2015 *Nat. Mater.* **14** 1013
[13] Deng K, Ding Y Q, He Z J, Zhao H P, Shi J and Liu Z Y 2009 *J. Phys. D* **42** 185505
[14] Torrent D and Sánchez-Dehesa J 2007 *New J. Phys.* **9** 323
[15] Peng S S, He Z J, Jia H, Zhang A Q, Qiu C Y, Ke M Z and Liu Z Y 2010 *Appl. Phys. Lett.* **96** 263502
[16] Zigoneanu L, Popa B I and Cummer S A 2011 *Phys. Rev. B* **84** 024305
[17] Li Y, Liang B, Tao X, Zhu X F, Zou X Y and Cheng J C 2012 *Appl. Phys. Lett.* **101** 233508
[18] Yuan B G, Tian Y, Cheng Y and Liu X J 2016 *Chin. Phys. B* **25** 104301
[19] Lu G X, Ding E L, Wang Y Y, Ping X Y, Cui J, Liu X Z and Liu X J 2017 *Appl. Phys. Lett.* **110** 123507
[20] Li Y, Liang B, Gu Z M, Zou X Y and Cheng J C 2013 *Sci. Rep.* **3** 2546
[21] Wang W Q, Xie Y B, Konneker A, Popa B I and Cummer S A 2014 *Appl. Phys. Lett.* **105** 101904
[22] Tang K, Qiu C Y, Ke M Z, Lu J Y, Ye Y T and Liu Z Y 2015 *Sci. Rep.* **4** 6517
[23] Mei J and Wu Y 2014 *New J. Phys.* **16** 123007
[24] Tian Y, Wei Q, Cheng Y, Xu Z and Liu X J 2015 *Appl. Phys. Lett.* **107** 221906
[25] Zhu Y F, Zou X Y, Li R Q, Jiang X, Tu J, Liang B and Cheng J C 2015 *Sci. Rep.* **5** 10966
[26] Yuan B G, Cheng Y and Liu X J 2015 *Appl. Phys. Express* **8** 027301
[27] Jahdali R A and Wu Y 2016 *Appl. Phys. Lett.* **108** 031902
[28] Fan X D, Zhu Y F, Liang B, Yang J and Cheng J C 2016 *Appl. Phys. Lett.* **109** 243501
[29] Gao H, Gu Z M, Liang B, Zou X Y, Yang J, Yang J and Cheng J C 2016 *Appl. Phys. Lett.* **108** 073501
[30] Wang X P, Wan L L, Chen T N, Song A L and Wang F 2016 *J. Appl. Phys.* **120** 014902
[31] Tian Y, Wei Q, Cheng Y and Liu X J 2017 *Appl. Phys. Lett.* **110** 191901
[32] Sánchez-Dehesa J, Angelov M I, Cervera F and Cai L W 2009 *Appl. Phys. Lett.* **95** 204102
[33] Liu C, Sun H X, Yuan S Q and Xia J P 2016 *Acta Phys. Sin.* **65** 044303 (in Chinese)
[34] Ge Y, Sun H X, Liu C, Qian J, Yuan S Q, Xia J P, Guan Y J and Zhang S Y 2016 *Appl. Phys. Express* **9** 066701
[35] Liu C, Sun H X, Yuan S Q, Xia J P and Qian J 2017 *Acta Phys. Sin.* **66** 154302 (in Chinese)
[36] Xia J P, Sun H X and Yuan S Q 2017 *Sci. Rep.* **7** 815
[37] Yu N F, Genevet P, Kats M A, Aieta F, Tetienne J P, Capasso F and Gaburro Z 2011 *Science* **334** 333